npj Computational Materials

www.nature.com/npjcompumats

ARTICLE OPEN

Number mismatch between cations and anions as an indicator for low lattice thermal conductivity in chalcogenides

Tingting Deng[1,2,3,6], Tian-Ran Wei[4,6], Hui Huang[1,2], Qingfeng Song[1], Kunpeng Zhao[4], Pengfei Qiu[1], Jiong Yang[5]✉, Lidong Chen[1,2,3] and Xun Shi[1,4]✉

Thermal conductivity is one of the most fundamental properties of materials with the value being determined by nearly all-scale structural features and multiple physical processes. Rapidly judging material's thermal conductivity is extremely important but challenging for the applications. The material genome paradigm offers a revolutionary way to efficiently screen and discover materials with designed properties by using accessible indicators. But such a performance indicator for thermal conductivity is quite difficult to propose due to the existence of multiple mechanisms and processes, especially for the materials with complex structures such as chalcogenides. In this study, the number mismatch between cations and anions is proposed as a practical performance indicator for lattice thermal conductivity in complex copper and silver chalcogenides, which can be used to explain the observed experimental data and find new low thermal conductivity materials. Such a number mismatch brings about rich phenomena to affect thermal conductivity including the complication of the unit cell and the creation of chemical hierarchy, point defects, rattling modes and lone-pair electrons. It is expected that this rich-connotation performance indicator can be also extended to other complex materials to discover designed thermal conductivities.

npj Computational Materials (2020)6:81 ; https://doi.org/10.1038/s41524-020-00355-x

INTRODUCTION

Thermal conductivity (κ) is a material's basic property that is used to characterize its heat conducting capability. High-κ materials are widely used in heat dissipating applications while low-κ ones are usually used in thermal insulation. In particular, thermal conductivity is one of the key parameters in thermoelectric materials. It also plays an important role in other energy conversion and storage materials such as solar cells and battery materials. Understanding thermal conductivity is thus of great significance in various disciplines. For semiconductors, heat conduction comes mainly from the vibration of lattice (phonons), i.e., the lattice thermal conductivity (κ_L)[1]. It is determined by heat capacity C_V, sound speed v and phonon relaxation time τ through the simplified relationship[2,3] $\kappa_L \propto C_V v^2 \tau$. The structures on atomic and/or unit cell levels basically decide the phonon dispersion, elastic properties, and the intensity of phonon–phonon normal and Umklapp scattering etc.[4,5], while the microstructures in all scales contribute additional boundaries, defects, and interfaces as phonon scattering centers[6]. The physical mechanisms on different levels have been developed to explain material's thermal conductivity observed in experiment. Particularly, a few conceptual directions have been proposed towards low κ_L, such as large cell with heavy atoms[1,7], small elastic parameters[8], and the existence of lone-pair electrons[9,10], soft bonds[8], rattling atoms[11], and liquid-like ions[12].

For the fields of thermoelectrics, design and discovery of new materials with low thermal conductivity is a key task. Materials genome initiative (MGI)[13] offers a revolutionary scenario to efficiently find new materials with desired properties[14], which is particularly suitable for thermal conductivity. MGI requires simple yet straightforward performance indicators for initial but fast high-throughput screening to pick up possible candidates. For lattice thermal conductivity, intuitive parameters such as average atomic mass (M) and primitive unit cell volume (V_{PUC}) are available in the database, but they are far below the requirements for materials with complex crystal structures and lattice dynamics. For example, in chalcogenides, chemical bonding inequality, and hierarchy are diverse, leading to various factors affecting thermal transport such as abundant intrinsic defects, loose bonding, lone-pair, and rattling atoms. They are likely to coexist and interact with each other. Thus, it is quite difficult to find simple performance indicators to quickly guide the thermal conductivity.

In this work, we report that the number mismatch (δ) between cations (N_{cation}) and anions (N_{anion}), $\delta = (N_{cation} - N_{anion})/N_{anion}$, can be regarded as the simple performance indicator to quickly and directly explain and discover materials with low lattice thermal conductivity (κ_L) in complex chalcogenides. Furthermore, new low-κ_L materials such as $Cu_2Sn_4S_9$ are screened by the proposed large number mismatch between cations and anions, and confirmed by experiment (Fig. 1).

RESULTS AND DISCUSSION

We go back to check the room-temperature lattice thermal conductivity of 73 complex ternary copper and silver chalcogenides (Fig. 1 and Supplementary Table 1). It ranges from 0.18 W m^{-1} K^{-1} in Ag_8GeTe_6 to 6.8 W m^{-1} K^{-1} in $CuInTe_2$, a quite large range. For each material, the δ value is calculated, and the room temperature κ_L varying with δ is shown in Fig. 1. Despite the diversity in composition and crystal structure, a clear decreasing

[1]State Key Laboratory of High Performance Ceramics and Superfine Microstructure, Shanghai Institute of Ceramics, Chinese Academy of Sciences, 200050 Shanghai, China. [2]Center of Materials Science and Optoelectronics Engineering, University of Chinese Academy of Sciences, 100049 Beijing, China. [3]School of Physical Science and Technology, ShanghaiTech University, 201210 Shanghai, China. [4]State Key Laboratory of Metal Matrix Composites, School of Materials Science and Engineering, Shanghai Jiao Tong University, 200240 Shanghai, China. [5]Materials Genome Institute, Shanghai University, 200444 Shanghai, China. [6]These authors contributed equally: Tingting Deng, Tian-Ran Wei
✉email: jiongy@t.shu.edu.cn; xshi@mail.sic.ac.cn

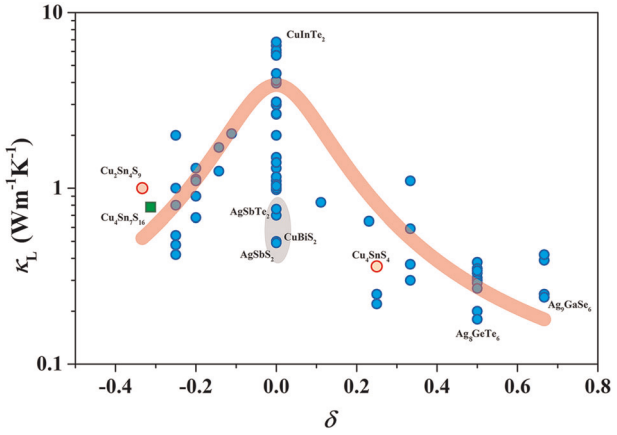

Fig. 1 Lattice thermal conductivity (κ_L) at room temperature varying with number mismatch between cations and anions (δ) in ternary Cu- and Ag-based chalcogenides. The red line is a guide to the eyes. The green square is $Cu_4Sn_7S_{16}$, which is used for the case study. $Cu_2Sn_4S_9$ and Cu_4SnS_4 (red circle) are the screened low κ_L materials based on proposed number mismatch between cations and anions. The raw data and the source for each material can be found in Supplementary Table 1.

trend of κ_L is observed when δ departs from 0, no matter whether the compounds are cation or anion rich. Particularly, all the materials with $|\delta| \geq 0.5$ have the κ_L values smaller than 0.5 W m^{-1} K^{-1}. As shown in Supplementary Fig. 1, the significant, negative correlation between κ_L and $|\delta|$ is quantified by the Spearman correlation coefficient $\rho_s = -0.79$, which is closer to -1 (totally negative relation) than either κ_L-M or κ_L-V_{PUC}. Furthermore, for each specific family of Cu-based materials, the decrease of normalized κ_L with $|\delta|$ is more straightforward (see Supplementary Fig. 2). These results strongly indicate that δ can be an effective performance indicator for low lattice thermal conductivity in Cu- and Ag-based complex chalcogenides. The detailed physical mechanisms for the low κ_L can be included in the simple parameter δ that can be immediately obtained from the chemical formula.

$Cu_4Sn_7S_{16}$: a case study

Here we pick up $Cu_4Sn_7S_{16}$ as a case study to show how the simple parameter δ can be a performance indicator for the low κ_L. Complex semiconductor $Cu_4Sn_7S_{16}$ is a largely distorted derivative of diamond-like compound with $\delta = -0.3125$[15]. As shown in Fig. 2a, $Cu_4Sn_7S_{16}$ exhibits a low $\kappa_L < 1$ W m^{-1} K^{-1} above room temperature, and the dependence of κ_L on T is quite weak, which is comparable with multiple-filled skutterudites[16] and Type-I clathrates[17].

There are a few reasons for such an observed low κ_L. Firstly and apparently, $Cu_4Sn_7S_{16}$ possesses a complex crystal structure. In this structure with the $R\bar{3}m$ ($Z = 3$) symmetry, sulfur atoms S1 (18 h), S2 (18 h), S3 (6c), and S4 (6c) constitute triangular, tetrahedral, and octahedral frameworks, accommodating Cu and Sn atoms[15] (Fig. 2d). This complex structure with diverse local structure units leads to a very large-cell volume (1695 Å^3) with 81 atoms per unit cell[15,18]. The primitive unit cell volume V_{PUC} is 565 Å^3 for $Cu_4Sn_7S_{16}$, which is considerably larger than typical diamond-like materials (V_{PUC} is 150–250 Å^3). Intuitively, a large and complex cell corresponds to numerous optical phonon modes (see Fig. 3d). These optical modes store a majority of heat (~78% at 20 K as shown in Fig. 2b) but exhibit a low group velocity while the acoustic modes contribute only ~20%. In addition, the optical modes may also suppress and even interact with the acoustic modes, thus suppressing the thermal transport.

Secondly, Cu1 atoms randomly occupy half of the 6c sites[15]. Therefore, high-density intrinsic vacancies are present and strongly scatter high-frequency phonons, reducing the κ_L by one order of magnitude (from 11.1 to 1.68 W m^{-1} K^{-1}) at room temperature (Fig. 2c).

Thirdly, our ab initio molecular dynamics (AIMD) simulations (Fig. 3a–c) and crystallographic data[19,20] show that Cu2 and Cu3 atoms exhibit a noticeably large vibration amplitude along *c*-axis and within *ab*-plane like rattling modes, respectively. These rattling-like behaviors lead to low-lying optical modes which start from as low as 2 meV and are intensely overlapped with the acoustic modes as indicated in Fig. 3d. In addition to altering the acoustic phonon dispersion near the boundary of Brillouin zone (particularly along Γ-A/L direction), the low-lying optical modes also introduce resonant scattering on acoustic phonons[21], further suppressing κ_L to 0.78 W m^{-1} K^{-1} at 300 K as shown in Fig. 2c. The reduction of κ_L is more directly demonstrated by the spectra data shown in Supplementary Fig. 3, where areas II and III are the contributions by point-defect scattering and resonant scattering, respectively.

As shown above, the large $|\delta|$ value in $Cu_4Sn_7S_{16}$ compound is unambiguously related to the low κ_L through the detailed physical mechanisms of large cell, rattling modes, and point defects. In fact, such a relationship can be easily extended to other materials. For example, Cu_3SbSe_3 has a large δ value of 0.33 and a low κ_L of 0.5–0.6 W m^{-1} K^{-1} at 300 K with the mechanisms of Cu rattling[11,25] and/or lone-pair electrons[9]. Similarly, tetrahedrite $Cu_{12}Sb_4S_{13}$ has a δ of 0.23 and a low κ_L about 0.65 W m^{-1} K^{-1} at room temperature[26,27]. All these detailed mechanisms of suppressing κ_L can be included in the simple performance indicator δ, which is schematically depicted in Fig. 4a, b and will be expanded in the next part.

Effects of δ on thermal transport

δ and large-cell effect. In chalcogenides, the relatively simple crystal structure cannot persist when $|\delta|$ is large enough. Thus, a larger cell with more atoms and lower symmetry tends to be adopted in order to accommodate the diverse bonding. In Fig. 4c, when $|\delta|$ is large, the primitive cell volume is large too. Although the data are scattered, the positive correlation between $|\delta|$ and V_{PUC} is quite clear. For large cells, the lattice complexity shrinks the first Brillouin zone and induces more optical modes. As a consequence, a majority of heat is damped in slowly propagating optical waves, and the acoustic branches are smothered or even interacted by the optical modes[4]. All these factors lead to the great reduction of κ_L.

δ and vacancies. Large δ means that certain crystallographic positions are not fully occupied. As an extreme case of point defects, vacancies have zero mass and free space to introduce large lattice fluctuation to scatter phonons. In fact, phonon scattering by point defects is a well-known strategy to reduce κ_L, which have been widely employed for a few dozens of years.

δ and local bonding distortion, rattling and lone pair. Large δ also brings about various local bonding distortions including the change in bond lengths and angles. Particularly, some atoms can be loosely bonded along certain directions or within certain planes, showing rattling-like vibrations to dramatically alter heat storage and transport. This effect has been demonstrated in the filled skutterudites[16,28], Cu_3SbSe_3[11], $Cu_{12}Sb_4S_{13}$[26], and Ag-based materials[8,29,30]. An extreme case of bonding inequality is the lone-pair electrons, which can further enhance the lattice anharmonicity[9,10]. Here we defined the microscopic distortion index Δ to qualitatively describe the degree of local chemical bond distortion, which is simply assumed as the sum of distortions in bond length Δ_l and bond angle Δ_θ. For most Cu-based ternary

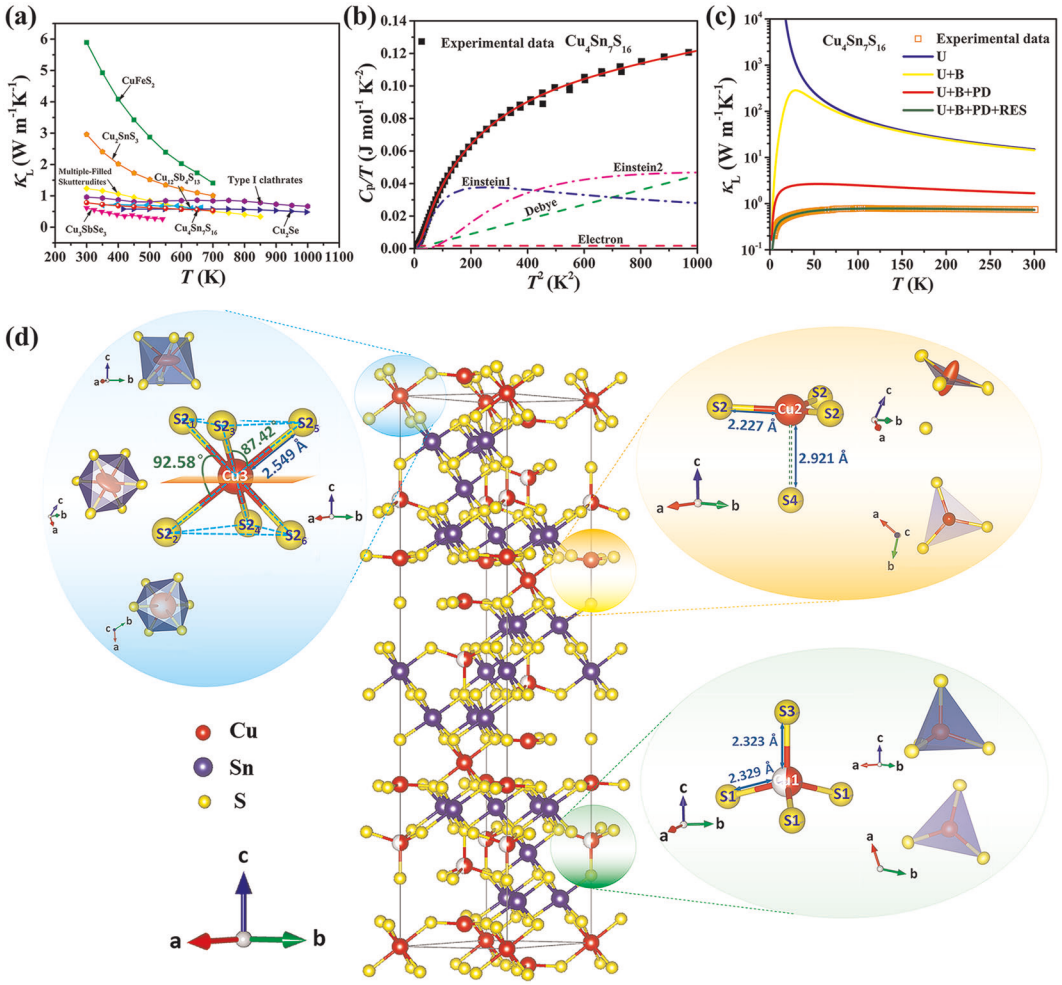

Fig. 2 Thermal transport properties and crystal structure for $Cu_4Sn_7S_{16}$. a κ_L as a function of temperature for various Cu-based chalcogenides. Data are taken from the followings: $CuFeS_2$ (ref.[22]), Cu_2SnS_3 (this work), skutterudites (ref.[16]), clathrates (ref.[17]), $Cu_{12}Sb_4S_{13}$ (ref.[23]), Cu_2Se (ref.[12]), Cu_3SbSe_3 (ref.[24]), and $Cu_4Sn_7S_{16}$ (this work, Supplementary Fig. 4). **b** C_p/T versus T^2 for $Cu_4Sn_7S_{16}$. The black squares are the experimental data. The red solid line represents the fitted curve by taking account the electronic, one Debye and two Einstein modes, which are shown by the dashed lines. Fitting parameters are given in Supplementary Table 2. **c** Phonon scattering mechanisms in $Cu_4Sn_7S_{16}$. U, B, PD, and RES denote the Umklapp process, grain-boundary scattering, point-defect scattering and resonant scattering, respectively. Fitting parameters are given in Supplementary Table 3. **d** Crystal structure of $Cu_4Sn_7S_{16}$ and local coordination of three types of Cu atoms.

chalcogenides, the cations are tetrahedrally or octahedrally bonded with anions in an ideal or distorted way. For the i^{th} cation coordination, it is defined

$$\Delta_l^i = (l_{max}^i - l_{min}^i)/l_{ideal}^i \quad (1)$$

$$\Delta_\theta^i = (\theta_{max}^i - \theta_{min}^i)/\theta_{ideal}^i, \quad (2)$$

where l_{max} and l_{min} are the largest and smallest bond lengths, respectively, and θ_{max} and θ_{min} are the largest and smallest bond angles, respectively. Here the data of ideally coordinated bonds are taken as the standard values. The detailed calculation method is described in Supplementary Fig. 5. For example, θ_{ideal} are 109.5° and 90° for tetrahedral and octahedral bonding, respectively. The total distortion degree of a material is the sum of the ones for each cation divided by the cation number:

$$\Delta = \sum_i (\Delta_l^i + \Delta_\theta^i)/N_{cation}. \quad (3)$$

For the case of lone pairs, it is assumed that the distance between the center cation and the lone pair is half of the normal bond length.

We calculated the Δ values based on the crystal structure of 19 Cu-based materials. Only 16 materials have the value of κ_L (Supplementary Table 4). As shown in Supplementary Fig. 6a, the lattice thermal conductivity exhibits a clear decreasing trend with Δ. The correlation between Δ and δ is relatively weak and scattered at the first sight (Supplementary Fig. 6b). Nonetheless, we found that this poor relativity is mainly caused by the treatment of vacancy-containing materials, in which the bonding between the anions and the virtue void is not included. After removing the five vacancy-containing materials ($Cu_4Sn_7S_{16}$, Cu_2SnSe_4, Cu_2GeS_4, Cu_4SnS_6, and $CuSn_{3.75}S_8$), the positive correction is clearly seen in Fig. 4d between the microscopic chemical bonding distortion parameter and the macroscopic ionic number mismatch. Thus, when δ deviates from 0, the degree to local chemical bond distortion is increased to greatly suppress κ_L.

κ_L-δ diagram in Cu–Sn–S family

Parameter δ is an effective indicator for κ_L in the materials with structural complexity and local bonding distortions. Large absolute value of δ means low κ_L. Thus the δ criterion can be used to discover low κ_L materials. Here we still take Cu–Sn–S family as the "material base" from the reported phase diagram[31]. It includes a variety of low-cost and environmentally friendly

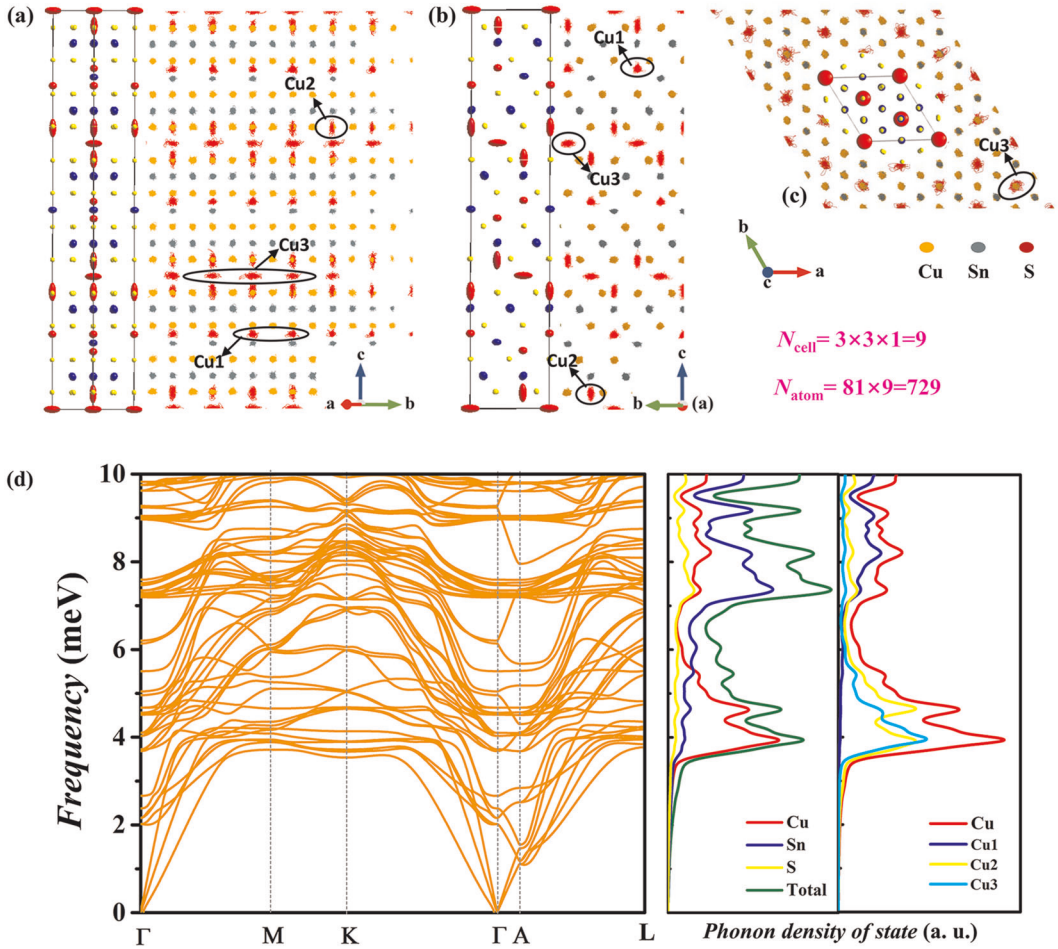

Fig. 3 Lattice dynamics of $Cu_4Sn_7S_{16}$. a–c Molecular dynamics trajectories for $Cu_4Sn_7S_{16}$; **d** Phonon dispersion and projected phonon density of states.

compounds and part of them can be potential candidates for various applications like thermoelectric, solar cells, and electrode materials. As shown in Fig. 5, the available experimental data (green symbols) of this family well follow the "δ criterion", further confirming the validity of this simple performance indicator. For the compounds[31] (the short vertical lines at the bottom of Fig. 5) without κ_L values being reported in the previous studies, the "δ criterion" suggests that $Cu_2Sn_2S_9$, $CuSn_{3.75}S_8$, $Cu_2Sn_4S_9$, $Cu_9Sn_2S_9$, and Cu_5SnS_4 are likely to exhibit low lattice thermal conductivities because of their large $|\delta|$ values. In experiment, we selected the nominally valence-state-balanced compound $Cu_2Sn_4S_9$ ($\delta = -0.33$) to check its κ_L. A low value of 1.0 $W\,m^{-1}\,K^{-1}$ is observed at room temperature, well consistent with our prediction. In addition, the compound Cu_4SnS_4 has a large δ of 0.25, but there are some discrepancies on the reported κ_L[32,33]. Particularly, Goto et al. reported a high value of 4 $W\,m^{-1}\,K^{-1}$[33], which is in contradictive with the "δ criterion". We rechecked this compound and found its κ_L at room temperature is 0.36 $W\,m^{-1}\,K^{-1}$, an extremely low value in chalcogenides. Furthermore, the κ_L data of the two compounds show weak dependences on temperature (Supplementary Fig. 14), which are in close analogy to $Cu_4Sn_7S_{16}$ with similarly large δ while in sharp contrast to Cu_2SnS_3. All the data have substantiated the effectiveness of the concise δ criterion in screening low-κ_L materials.

Limitations of δ

There are certainly some limitations for this simple indicator. Fundamentally, the case of $\delta = 0$ is pre-assumed to be the tetrahedrally bonded diamond-like semiconductors. The real case is more complicated. A typical example for this deviation is the Sb/Bi-containing compounds (e.g., $CuBiS_2$ and $AgSbS_2$), where the lone-pair electrons of Sb/Bi make the structure largely different from the chalcopyrite despite the same 1–1–2 composition. This is the main reason why the κ_L data are largely scattered for $\delta = 0$ (Fig. 1). In addition, the mismatch criterion does not consider the difference in atomic mass. Therefore, this indicator is more effective and reliable for homologs, i.e., a family of compounds with the same elements but different compositions. A good demonstration has been shown above for the Cu–Sn–S materials.

In real applications, the total thermal conductivity is of greater interest. We found that most Cu/Ag-based ternary chalcogenides have extremely low κ_e (<5% of κ_{total}) at room temperature. Also, there seems no clear correlation between κ_e and $|\delta|$. However, things can be more complicated when κ_e is nonnegligible in other systems, and the possible relationship between κ_e and $|\delta|$ needs further investigation.

In summary, this work proposed that the mismatch (δ) between the number of cations and anions is a practical performance indicator for low κ_L in ternary Cu- and Ag-based chalcogenides. When the mismatch exists, multiple phenomena and effects such as large cell, point defects, chemical bonding distortion and inequality, rattling atoms and lone pair may be induced to lower κ_L. This criterion and the underlying mechanisms have been illustrated in the $Cu_4Sn_7S_{16}$ compound and well extended to other ternary Cu- and Ag-based chalcogenides. Guided by the κ_L-δ relationship, low-κ_L $Cu_2Sn_4S_9$ compound was predicted and confirmed. Such an intuitive indicator provides a unique

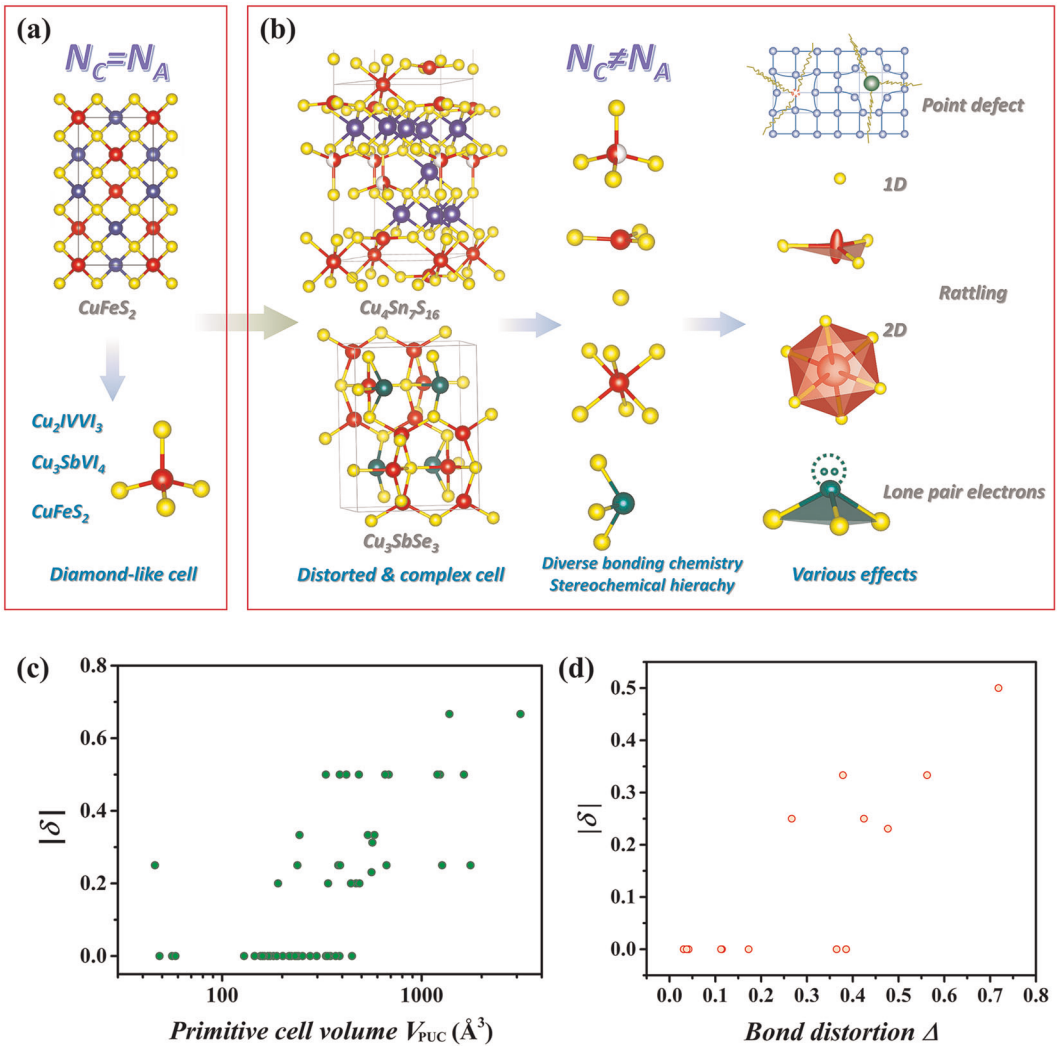

Fig. 4 Mechanisms of ionic number mismatch influencing thermal transport. a, **b** Schematic depiction of the effects of number mismatch between cations and anions on thermal transport in Cu-based chalcogenides. Ionic number mismatch varying with **c** primitive cell volume for Cu- and Ag-based compounds and **d** local bond distortion for Cu-based compounds.

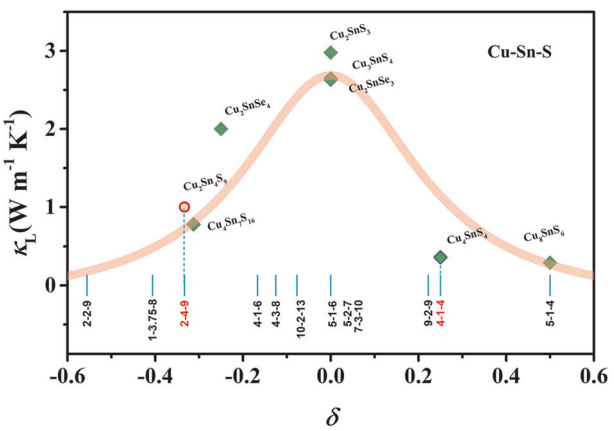

Fig. 5 κ_L-δ diagram for the Cu–Sn–S compounds. The squares are the experimental data. The red line is fitted to guide the eyes. The short vertical line donates the mismatch of various Cu–Sn–S compounds from the reported phase diagram[31] whose lattice thermal conductivity has not been reported. Materials with large $|\delta|$ values are expected to exhibit low κ_L.

perspective for understanding thermal transports and is powerful for efficiently screening and designing low κ_L materials for energy conversion and thermal management applications.

METHODS

Synthesis

$Cu_4Sn_7S_{16}$, Cu_2SnS_3, Cu_4SnS_4, and $Cu_2Sn_4S_9$ polycrystalline samples were synthesized by different methods with the details described in Supplementary Information.

Characterization

The phase purity and crystal structure were detected by X-ray diffraction with Cu K_α X-ray sources (XRD, Rigaku D/max 2550 V). The elemental distribution was characterized by scanning electron microscopy (ZEISS supra 55) and energy dispersive X-ray spectroscopy (Oxford) with accelerate voltage set as 20 kV. Samples' phase purity and homogeneity are shown in Supplementary Figs. 7–13. High-temperature thermal conductivity was derived from the formula $\kappa = \rho C_P \lambda$, where ρ is the density, C_P is the heat capacity calculated by Dulong–Petit law, and λ is thermal diffusivity measured between 300 and 700 K by using the laser flash method (LFA 457, NETZSCH). Low-temperature C_P and κ_L were measured by Physical Property Measurement System (PPMS Quantum Design). The uncertainty for κ_L is within 10%.

Computation

The AIMD was performed for $Cu_4Sn_7S_{16}$ at 300 K. A large supercell, $3 \times 3 \times 1$ of the 81-atom unit cell (729 atoms in total), was constructed for the AIMD. The simulation time was over 18 ps with a step of 2 fs. The AIMD was carried out by the Vienna ab initio simulation package[34], with the projector augmented wave method[35] and Perdew–Burke–Ernzerhof generalized gradient approximation functional[36]. The temperature dependent effective potential method[37,38] was adopted to extract the harmonic interatomic force constants and phonon dispersions from the AIMD trajectories and forces.

DATA AVAILABILITY

The data supporting the findings of this study are available within the main text and its Supplementary Information files and are available from the corresponding authors upon reasonable request.

Received: 26 February 2020; Accepted: 4 June 2020;
Published online: 23 June 2020

REFERENCES

1. Berman, R. *Thermal Conduction in Solids*. (Clarendon Press, 1976).
2. Toberer, E. S., Baranowski, L. L. & Dames, C. Advances in thermal conductivity. *Annu. Rev. Mater. Res.* **42**, 179–209 (2012).
3. Yang, J. in *Thermal Conductivity: Theory, Properties and Applications* (ed Terry, M. Tritt) Ch. 1.1, 1–20 (Plenum, 2004).
4. Toberer, E. S., Zevalkink, A. & Snyder, G. J. Phonon engineering through crystal chemistry. *J. Mater. Chem.* **21**, 15843–15852 (2011).
5. Chen, Z., Zhang, X. & Pei, Y. Manipulation of phonon transport in thermoelectrics. *Adv. Mater.* **30**, 1705617 (2018).
6. Biswas, K. et al. High-performance bulk thermoelectrics with all-scale hierarchical architectures. *Nature* **489**, 414–418 (2012).
7. Slack, G. A. The thermal conductivity of nonmetallic crystals. *Solid State Phys.* **34**, 1–71 (1979).
8. Lin, S. et al. High thermoelectric performance of Ag_9GaSe_6 enabled by low cutoff frequency of acoustic phonons. *Joule* **1**, 1–15 (2017).
9. Skoug, E. J. & Morelli, D. T. Role of lone-pair electrons in producing minimum thermal conductivity in nitrogen-group chalcogenide compounds. *Phys. Rev. Lett.* **107**, 235901 (2011).
10. Nielsen, M. D., Ozolins, V. & Heremans, J. P. Lone pair electrons minimize lattice thermal conductivity. *Energy Environ. Sci.* **6**, 570–578 (2013).
11. Qiu, W. et al. Part-crystalline part-liquid state and rattling-like thermal damping in materials with chemical-bond hierarchy. *Proc. Natl Acad. Sci. USA.* **111**, 15031–15035 (2014).
12. Liu, H. et al. Copper ion liquid-like thermoelectrics. *Nat. Mater.* **11**, 422–425 (2012).
13. de Pablo, J. J. et al. New frontiers for the materials genome initiative. *npj Comput. Mater.* **5**, 41 (2019).
14. Xi, L. et al. Discovery of high-performance thermoelectric chalcogenides through reliable high-throughput material screening. *J. Am. Chem. Soc.* **140**, 10785–10793 (2018).
15. Chen, X.-a, Wada, H., Sato, A. & Mieno, M. Synthesis, electrical conductivity and crystal structure of $Cu_4Sn_7S_{16}$ and $Cu_{12}Sb_4S_{13}$. *J. Solid State Chem.* **139**, 144–151 (1998).
16. Shi, X. et al. Multiple-filled skutterudites: high thermoelectric figure of merit through separately optimizing electrical and thermal transports. *J. Am. Chem. Soc.* **133**, 7837–7846 (2011).
17. Shi, X. et al. On the design of high-efficiency thermoelectric clathrates through a systematic cross-substitution of framework elements. *Adv. Funct. Mater.* **20**, 755–763 (2010).
18. Deng, T. et al. Thermoelectric properties of n-type $Cu_4Sn_7S_{16}$-based compounds. *RSC Adv.* **9**, 7826–7832 (2019).
19. Lemoine, P. et al. High temperature neutron powder diffraction study of the $Cu_{12}Sb_4S_{13}$ and $Cu_4Sn_7S_{16}$ phases. *J. Solid State Chem.* **247**, 83–89 (2017).
20. Jemetio, J. P. F., Zhou, P. & Kleinke, H. Crystal structure, electronic structure and thermoelectric properties of $Cu_4Sn_7S_{16}$. *J. Alloy. Compd.* **417**, 55–59 (2006).
21. Pohl, R. O. Thermal conductivity and phonon resonance scattering. *Phys. Rev. Lett.* **8**, 481–483 (1962).
22. Li, Y. et al. Thermoelectric transport properties of diamond-like $Cu_{1-x}Fe_{1+x}S_2$ tetrahedral compounds. *J. Appl. Phys.* **116**, 203705 (2014).
23. Kosaka, Y. et al. Effects of Ge and Sn substitution on the metal–semiconductor transition and thermoelectric properties of $Cu_{12}Sb_4S_{13}$ tetrahedrite. *Phys. Chem. Chem. Phys.* **19**, 8874–8879 (2017).
24. Wei, T.-R., Wu, C.-F., Sun, W., Pan, Y. & Li, J.-F. Is Cu_3SbSe_3 a promising thermoelectric material? *RSC Adv.* **5**, 42848–42854 (2015).
25. Qiu, W., Wu, L., Ke, X., Yang, J. & Zhang, W. Diverse lattice dynamics in ternary Cu-Sb-Se compounds. *Sci. Rep.* **5**, 13643 (2015).
26. Lai, W., Wang, Y., Morelli, D. T. & Lu, X. From bonding asymmetry to anharmonic rattling in $Cu_{12}Sb_4S_{13}$ tetrahedrites: when lone-pair electrons are not so lonely. *Adv. Funct. Mater.* **25**, 3648–3657 (2015).
27. Suekuni, K. et al. Retreat from stress: rattling in a planar coordination. *Adv. Mater.* **30**, e1706230 (2018).
28. Sales, B., Mandrus, D. & Williams, R. K. Filled skutterudite antimonides: a new class of thermoelectric materials. *Science* **272**, 1325–1328 (1996).
29. Jiang, B. et al. An argyrodite-type Ag_9GaSe_6 liquid-like material with ultralow thermal conductivity and high thermoelectric performance. *Chem. Commun.* **53**, 11658–11661 (2017).
30. Tan, G., Hao, S., Zhao, J., Wolverton, C. & Kanatzidis, M. G. High thermoelectric performance in electron-doped AgBi3S5 with ultralow thermal conductivity. *J. Am. Chem. Soc.* **139**, 6467–6473 (2017).
31. Fiechter, S., Martinez, M., Schmidt, G., Henrion, W. & Tomm, Y. Phase relations and optical properties of semiconducting ternary sulfides in the system Cu–Sn–S. *J. Phys. Chem. Solids* **64**, 1859–1862 (2003).
32. Choudhury, A. et al. New insights into the structure, chemistry, and properties of Cu_4SnS_4. *J. Solid State Chem.* **253**, 192–201 (2017).
33. Goto, Y., Kamihara, Y. & Matoba, M. Effect of indium substitution on the thermoelectric properties of orthorhombic Cu_4SnS_4. *J. Electron. Mater.* **43**, 2202–2205 (2014).
34. Kresse, G. & Furthmüller, J. Efficient iterative schemes for ab initio total-energy calculations using a plane-wave basis set. *Phys. Rev. B* **54**, 11169–11186 (1996).
35. Blöchl, P. E. Projector augmented-wave method. *Phys. Rev. B* **50**, 17953–17979 (1994).
36. Perdew, J. P., Burke, K. & Ernzerhof, M. Generalized gradient approximation made simple. *Phys. Rev. Lett.* **77**, 3865–3868 (1996).
37. Hellman, O., Abrikosov, I. & Simak, S. Lattice dynamics of anharmonic solids from first principles. *Phys. Rev. B* **84**, 180301 (2011).
38. Hellman, O. & Abrikosov, I. A. Temperature-dependent effective third-order interatomic force constants from first principles. *Phys. Rev. B* **88**, 144301 (2013).

ACKNOWLEDGEMENTS

This work is supported by the National Key Research and Development Program of China (2018YFB0703600), the National Natural Science Foundation of China (51625205, 91963208, and 51802333), the Key Research Program of Chinese Academy of Sciences (KFZD-SW-421) and the Youth Innovation Promotion Association of CAS (2016232).

AUTHOR CONTRIBUTIONS

T.D. and T.-R.W. contributed equally to this work. T.-R.W., J.Y., and X.S. proposed the idea and designed the experiments. T.D. performed material syntheses, sample measurements, and data collection. T.D. and T.-R.W. analyzed the data. J.Y. and H.H. performed the ab initio molecular dynamics (AIMD) calculations. T.D. and T.-R.W. wrote the papers with the guidance of J.Y., X.S., and L.C. All authors discussed the results and commented on the paper.

COMPETING INTERESTS

The authors declare no competing interests.

ADDITIONAL INFORMATION

Supplementary information is available for this paper at https://doi.org/10.1038/s41524-020-00355-x.

Correspondence and requests for materials should be addressed to J.Y. or X.S.

Reprints and permission information is available at http://www.nature.com/reprints

Publisher's note Springer Nature remains neutral with regard to jurisdictional claims in published maps and institutional affiliations.